

Technical note

A rigid body model of the forearm

Johannes Reich*, Wolfgang J. Daunicht

Neurologisches Therapiezentrum, Hohensandweg 37, D- 40591 Düsseldorf, Germany

Accepted 2 February 2000

Abstract

In this article the forearm, with its complex, continuous motion of masses during pronation/supination, was approximated by a rigid body model consisting of a radial segment rotating around an ulnar segment. The method used to obtain the model parameters is based on three-dimensional voxel data that include velocity information. We propose a criterion that allows the voxels to be attributed to either of the two segments. It is based on the notion that the rotational kinetic energy determined from the voxel data equals the kinetic energy of the rigid body model. To obtain a three-dimensional smoothing we further propose a parameterization of the shape of both segments. These shapes can then be used to determine the dynamic integrals of the segments, i.e. mass, center of mass, and inertia. Using this approach we determined all model parameters for a human forearm from three series of MRI scans in a supinated, a pronated, and an intermediate position. In the appendix, a procedure is described that allows the dynamic quantities to be scaled homogeneously without recalculation of the integrals. Thus, this article provides all essential parameters required for three-dimensional dynamic simulations of general movements of the forearm. © 2000 Elsevier Science Ltd. All rights reserved.

Keywords: Human; Forearm; Rigid body; Model; Dynamic simulation; Scaling

1. Introduction

The dynamic modelling of the human forearm, and the pronation–supination (PS) movement, in particular, have been treated less than adequately in the biomechanics literature. Most authors thus far were concerned with the kinematics rather than the dynamics of the PS of the human forearm. An early extensive qualitative discussion can be found in Fick (1911). The modern studies of this subject have been motivated mostly by interest in the development of forearm prostheses. Chao and Morrey (1978) investigated the position of the rotational axes of the forearm using an orthogonal X-ray technique. They identified the axis of the flexion/extension (FE) of the elbow as the center of the humeral trochlea and showed that the ulna was fixed for the PS. Youm et al. (1979) used an LED-technique to quantify the forearm motion. They determined the PS-axis along the straight line between the center of the proximal caput radii and the distal center of the ulna; and the FE-axis as the center of the humeral trochlea, independent on the rotation angle.

Robin et al. (1986) used a fast computed-tomography technique to analyze the angle and the distance between the ulna and radius during the PS, but they did not give any data concerning the movements of the masses of the forearm during the rotation. An et al. (1981) determined several physiological parameters like moment arms, volumes and physiological cross sections for the muscles spanning the elbow. This investigation was supplemented by a study by Murray et al. (1995), who measured the dependence of the moment arms of these muscles on both the FE and the PS, and compared these data to a kinematic model, based on finite-element bones of the Viewpoint Company.

To our knowledge, in previous approaches to forearm dynamics a single rigid segment was used that rotated around two axes through the elbow joint (Hatze, 1980; Winter, 1990; Nigg and Herzog, 1999). Peterson (1994) presented a rigid body model of the arm, but he neither gave any data concerning the dynamical parameters of his model, nor mentioned the methods with which such parameters were determined.

A single rigid body approximation is sufficient for studies of arm kinematics, of moment equilibrium situations, and of pure flexion/extension. However, for general dynamic simulations of arm movements, in particular with rapid PS components, the inertia of the

* Corresponding author. Tel.: + 49-211-78160; fax: + 49-211-784353.

E-mail address: reich@uni-duesseldorf.de (J. Reich).

forearm must be modelled using at least two segments. Otherwise, it is to be expected that the inertia and consequently the torques related to the PS will be grossly overestimated. Such a distinction between segments also allows the effects of muscles between humerus and ulna to be correctly modelled, as the ulna has only one degree of freedom instead of two. Obviously, the effects of muscles located between radius and ulna (*M. pronator quadratus*) cannot be modelled without making such a distinction.

The aim of the present study was to develop a method to approximate the continuum dynamics of the forearm using two rigid bodies in such a way as (a) to obtain reasonably accurate inertias for all kinds of movements and (b) to estimate the accuracy of the resulting model. Based on MRI scans (Martin et al., 1989), the forearm was partitioned into two segments: an ulnar segment that articulates with the humerus in the elbow joint in one degree of freedom, and a radial segment that articulates with the ulnar segment around the PS-axis. The resulting kinematic and dynamic parameters of both segments of the forearm (mass, center of mass, and inertia tensor) of a young male adult are presented.

To extend the range of application of our data, a method is required for scaling the presented forearm parameters with respect to different forearm geometries. To this purpose, in the appendix a linear scaling procedure is described.

2. Methods

2.1. Recording of 3 series of MRI-scans

Our analysis was based on three series of t2-weighted MRI-scans of the forearm of one 29 year old male subject. The subject gave his informed consent to the procedure. The resolution of the MRI-scan was 0.55 mm in the slice plane, i.e. 256 pixel of the MRI-scan corresponded to 14 cm. Each series was limited to 22 slices 1 cm apart. The skin was marked in order to put the elbow approximately at the same position in each series. The scans covered most of the forearm, approximately from the radial tuberositas to the ulnar incisure. Series 1 was taken in supinated, Series 3 in a pronated and Series 2 in an intermediate position. The exact PS-angle of the positions was determined from the scans (see results).

To use the ulna as the common body of reference for all three series, the longitudinal displacement was reduced further to less than 0.5 cm by omitting the first slice of the supinated and intermediate series and the last slice of the pronated series such that the remaining 21 successive scans of each series had the best correspondence. The transversal and rotational misalignments were minimized by rotating and translating numerically the slices of the supinated and pronated series based on a linear longitudinal parametric fit.

Of the remaining 3×21 scans, every 4th one was selected for further evaluation, resulting in 6 scans of each series, 4 cm apart, renumbered 2, 6, ..., 22 from distal to proximal. The resulting superposition of the six scans of all three series is presented in Fig. 1

As the distance between the olecranon and the processus styloideus of the ulna (26 cm) exceeded the size of the MRI coil for high-resolution scans (23 cm), it was not possible to include the humero-ulnar and the radio-carpal joint in the scans of the forearm. To determine the points and axes of articulation between forearm, humerus, and hand, it was therefore necessary to fit a bone polygon set of the arm bones (Viewpoint Company) to the bony surfaces determined in the 22 scans of the supinated series. The joint axes of the bone polygon set were determined by repeatedly fitting the shape, orientation, and position or rotational surfaces to the surfaces of the trochlea and the ossa carpi of the bone polygon set using a visually guided iterative procedure.

2.2. Quantifying the movement of the tissue

As an example, the movement of the forearm tissue between slice 2 of the pronated series and slice 2 of the intermediate series is shown in Fig. 2.

To quantify such movements, we approximated the nonlinear mapping M_i of the supinated onto the intermediate series ($i = 1$) and the pronated onto the intermediate series ($i = 2$). This was done under visual supervision by local rotation and translation of small square areas of one slice of the supinated and pronated series, respectively, onto the corresponding slice of the intermediate series, so that characteristic local structures were brought into congruence.

The x - and y -component of the mapping corresponding to Fig. 2 are shown in Fig. 3. For small areas, where no characteristic local structures could be found, the mappings were interpolated by means of a two-dimensional polynomial fit of third order.

The PS-axis was determined by fitting circles to the joint surfaces of radius and ulna of the superpositioned slices 2 and 22 of all 3 series. The intersections of the PS-axis with the intermediate slices were calculated by interpolation.

With the knowledge of the mappings M_i of the tissue and of the rotational axis, the local rotation of each voxel $\Delta\alpha_i = \Delta\alpha_i(x, y, z)$ relative to this axis could be calculated for both mappings. x and y are the horizontal and vertical coordinates in the slice planes, and z is measured in the direction orthogonal to the slice planes. To determine the rotational angles $\Delta\alpha_i^0$ between the radius and the ulna, only voxels representing bony tissue were used.

The PS-axis differed from the orthonormal of the slice by a skew angle of 10.9° . Thus the mapping actually relied on the assumption that the pixels belong to longitudinal structures parallel to the PS-axis. The small angle

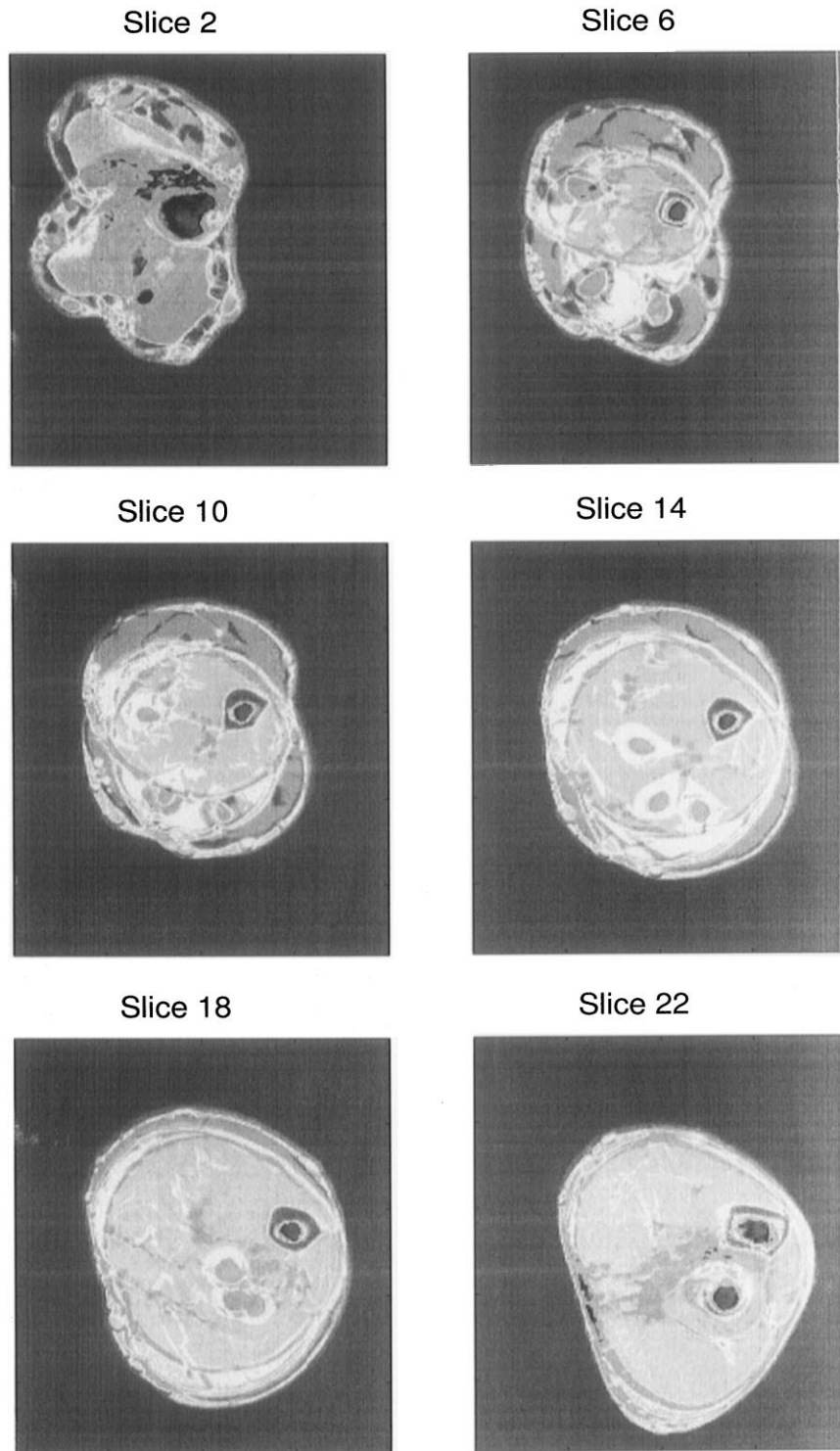


Fig. 1. Superposition of the three MRI-series after translation and rotation of the supinated and pronated series so that the ulna remained invariant by PS in all three series. Shown are the slices 2, 6, 10, 14, 18, and 22 in intervals of 4 cm. Slice 2 (distal) cuts the forearm slightly proximal to the tuberositas radii. Slice 22 (proximal) cuts the forearm slightly distal to the incisura ulnaris of the radius.

error introduced by projecting the circular movement under the skew angle was neglected. The effect of this error could be estimated by the comparison of the results of the partition by both mappings (see discussion).

2.3. Voxel-based partitioning into two distinct segments

The partitioning of the forearm masses into a radial and an ulnar segment marks the transition from

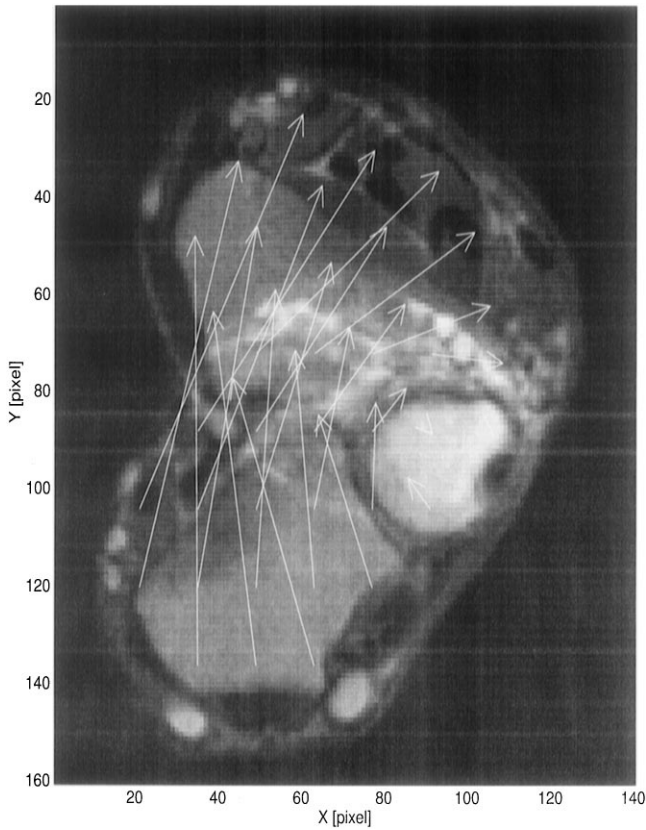


Fig. 2. Vector-plot of the mapping of slice 2 of the pronated series onto slice 2 of the intermediate series.

a continuum to a rigid body model. The basic idea for this partitioning was to postulate that the kinetic energy (of a slow rotation around the PS-axis) of the continuum case, which could be determined by the mappings, should equal the kinetic energy of the rigid body case — still to be determined.

This partitioning was done for both mapping separately, so that a comparison of the resulting two partitions allowed an assessment of the soundness of the rigid body assumption over a broad range of PS-angles.

In general, the rotational Kinetic energy E_{kin} of a mechanical system is given by

$$E_{kin} = \frac{1}{2} \int_m (\omega \times \mathbf{r})^2 dm = \frac{1}{2} \int_m \omega^2 r_{\perp}^2 dm, \tag{1}$$

where ω is the angular velocity vector of the mass element dm at the position \mathbf{r} . ω is the magnitude of ω , and r_{\perp} is the length of the perpendicular distance from \mathbf{r} to the axis. The origin of the coordinate system is placed on the axis.

The distance ξ of the voxels to the axis was measured in the slice planes. With β defined as the angle between the slice planes and the PS-axis, $\xi = r_{\perp}/(\sin \beta)$ holds true. We assume that ω is linearly related to the rotational angle $\Delta\alpha$, i.e. that $\omega = \Delta\alpha/\Delta t$.

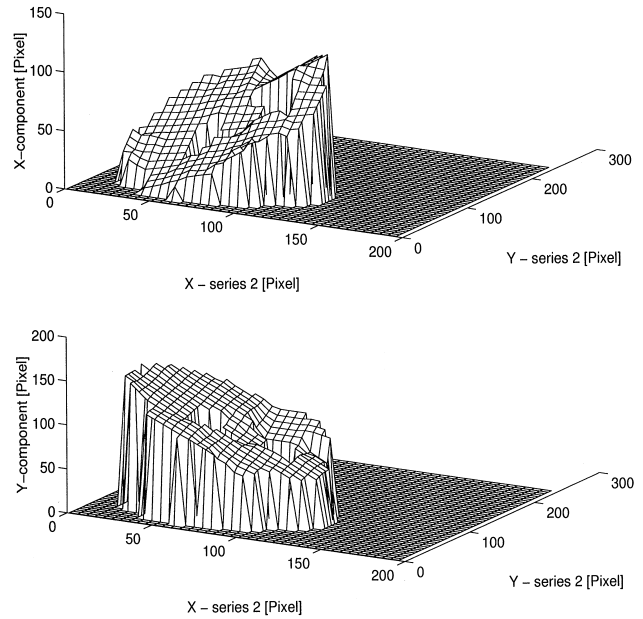


Fig. 3. X- and Y-component of the mapping of slice 2 of the pronated series onto slice 2 of the intermediate series before interpolation of the areas without characteristic structures. The relative smoothness of the mapping is demonstrated.

Now, E_{kin} has to be calculated for the movement determined by the mappings, i.e. with $\Delta\alpha = \Delta\alpha(x, y, z)$ depending on the voxel position. In contrast, in a true rigid body all $\Delta\alpha$ were identical for a single segment, i.e. $\Delta\alpha = \Delta\alpha^0$ for the radial and $\Delta\alpha = 0$ for the ulnar segment. As most of the tissue will move less than the angle of the radial bone $\Delta\alpha^0$, the assumption that a voxel of the soft tissue belongs to the radial segment will in general overestimate its kinetic energy. The overestimation can be compensated by attributing only a fraction of the soft tissue to the radial segment. It seems sound to select only those parts which contribute most to the kinetic energy of the radial segment. Thus the requirement that the kinetic energies of the continuum and of the rigid body case should be equal provides an implicit equation for the unknown cut-off value $g_{cut-off}$ of the individual contribution of each voxel to the kinetic energy.

More formally, this is written as follows:

$$E_{kin}^{cont.} \stackrel{!}{=} E_{kin}^{radial\ seg.} \tag{2}$$

or

$$\frac{1}{2} \int_{forearm} \left(\frac{\Delta\alpha(x, y, z)}{\Delta t} \right)^2 \left(\frac{\xi}{\sin \beta} \right)^2 \rho dV \stackrel{!}{=} \frac{1}{2} \int_{radial\ seg.} \left(\frac{\Delta\alpha^0}{\Delta t} \right)^2 \left(\frac{\xi}{\sin \beta} \right)^2 \rho dV. \tag{3}$$

The common factor $\rho/2(\Delta t \sin \beta)^2$ of both sides can be eliminated. The resulting terms are proportional to E_{kin} and were denoted as $G^{cont.}$ and $G^{radial\ seg.}$. Writing the integrals as sums over the voxel data this reads

$$G^{cont.} := \sum_k^{all\ voxels} g_k(\xi_k, \Delta\alpha_k = \Delta\alpha(x, y, z)),$$

$$G^{radial\ seg.} := \sum_k^{gk > g_{cut-off}} g_k(\xi_k, \Delta\alpha_k = \Delta\alpha^0) \tag{4}$$

with the index k indicating the voxels. The contribution of the k th voxel to G is defined as $g_k := (\Delta\alpha_k)^2 \xi_k^2$. This resulted in a dependence of $G^{radial\ seg.}$ on the cut-off value, i.e. $G^{radial\ seg.} = G^{radial\ seg.}(g_{cut-off})$ and $g_{cut-off}$ was given implicitly by condition

$$G^{cont.} \stackrel{!}{=} G^{radial\ seg.} \tag{5}$$

2.3.1. Comparison of the two mappings

Actually, the resulting g_k , G and $g_{cut-off}$ depended on the mapping M_i . The difference between G_1 and G_2 should allow for a consistency check of the partition of the forearm and, therefore, of the description of the PS by a model of rigid bodies.

If both partitions were identical, the following relation would hold true:

$$G_1 = \left(\frac{\Delta\alpha_1^0}{\Delta\alpha_2^0}\right)^2 G_2. \tag{6}$$

Actually, the measured value of G_1 was only 5.8% larger than $(\Delta\alpha_1^0/\Delta\alpha_2^0)^2 G_2$.

2.3.2. Parameterization of the partition

In order to minimize the discretization error and to obtain a unique model of the forearm, we propose a parameterization of the surfaces of both voxel-based partitions. This parameterization description was then used in a numerical Monte-Carlo-integration procedure to calculate the relevant integrals.

The surface ε of the forearm of series 2 was explicitly parameterized by a family of rotated and deformed ellipses

$$\varepsilon = \varepsilon(\delta, z)$$

$$= \left(\begin{pmatrix} p_x \\ p_y \end{pmatrix} + \begin{pmatrix} \cos \alpha & \sin \alpha \\ -\sin \alpha & \cos \alpha \end{pmatrix}_z \begin{pmatrix} (\cos(\delta) + \varepsilon|\cos(\delta)|)a_x \\ \sin(\delta)a_y \end{pmatrix} \right), \tag{7}$$

where $\delta \in [0, 360^\circ]$ and $z \in [0.5, 26.5]$. The integer values of z corresponded to the slice index. The parameters p_x , p_y , a_x , a_y , α , and ε depended on z , and were determined for the slices 2, 6, ..., 22 of the intermediate series and fitted by second-order polynomials.

For the parameterization of the intersegmental border an implicit approach was used. We defined an auxiliary function $\Phi = \Phi(x, y, z)$,

$$\Phi(x, y, z) = \frac{1}{\left| \begin{pmatrix} x \\ y \end{pmatrix} - q_1(z) \right|} - \frac{1}{\left| \begin{pmatrix} x \\ y \end{pmatrix} - q_2(z) \right|}, \tag{8}$$

where (x, y) measured the directions in the plane of the slices, $z \in [0.5, 26.5]$, q_1 corresponded to the PS-axis, and q_2 ran parallel to that. Each position \mathbf{r} with a $\Phi(x, y, z)$ larger than a $\Phi_{cut-off}(z)$ — still to be determined — was defined as belonging to the radial segment. The partition-parameter $\Phi_{cut-off}(z)$ was found for the slices 2, 6, ..., 22 by the requirement, that the masses of the segments resulting from the voxel-based partition should equal those from the model-based partition.

Voxels with $\Phi > \Phi_{cut-off}$ could be identified only in slices with an index $i \leq 14$. As an approximation of the function $\Phi_{cut-off}(z)$ a rational function with a pole at $z = 18$ was therefore fitted to the data of both mappings.

The difference of the number of voxels with $\Phi > \Phi_{cut-off}$, as a measure for the range of validity of the method, was 4.6% between the two mappings. The difference of the number of voxels between the parameterized model and the voxel-based criterion, i.e. the fraction of voxels that were placed in the opposite segment because of the parameterization, was less than 6.8% for both mappings.

The voxel and model-based partitions as well as the parameterization of the surface of the forearm for the slices 2, 6, ..., 22 resulting from the mapping M_1 are shown in Fig. 4.

2.4. Defining and referencing the coordinate systems

To relate the quantities of the ulna and radius to the other segments of the kinematic chain of the arm, i.e. the upper arm and the hand, the coordinates and direction of the elbow joint axis and the center of rotation of the hand-joint axis have to be known.

In defining an anatomical coordinate system, one has to decide whether to use bony landmarks, which would simplify the determination of the coordinate system in vivo, or rotational axes and joint centers, which would simplify its usage in a computer model. Because of our interest in this study to provide data for numerical simulations of the PS, we opted for the functional approach and defined the anatomical coordinate systems as follows (cf. Chadwick et al., 1996):

- Ulna:*
- Origin: center of the trochlea
- z-axis: defined by the origin and the center of the (distal) ulnar head.
- The direction is from distal to proximal

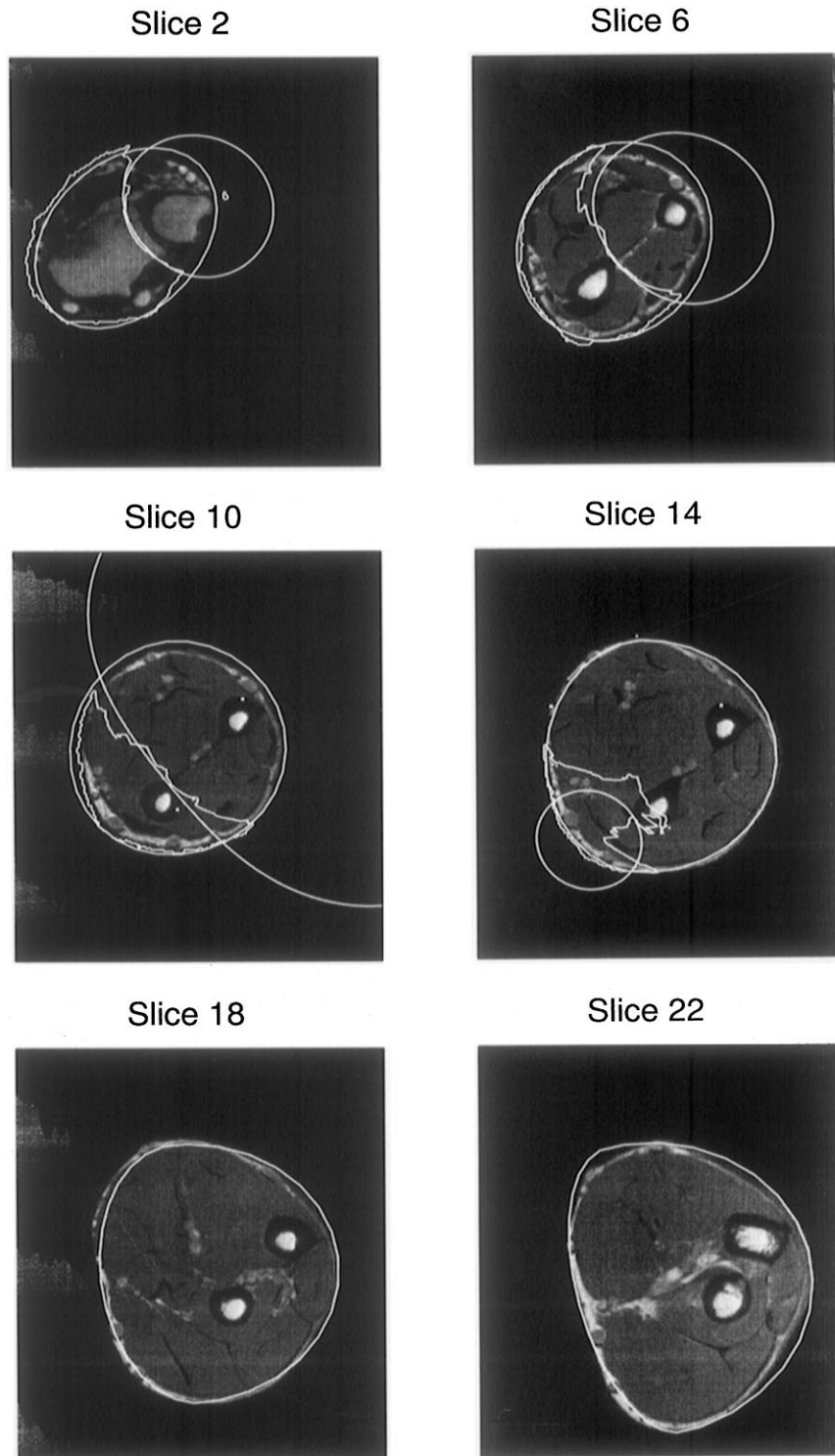


Fig. 4. Segmental partitioning of the forearm with the mapping of the pronated onto the intermediate series. The irregular border in the slices 2, 6, 10, and 14 result from the voxel-based partition of the segments. The smooth curves represent the parameterized surface of the forearm and the parameterized partition of both segments corresponding to Eq. (7) and (8) with the respective $\Phi_{\text{cut-off}}$.

x-axis: orthogonal to the *z*-axis and in the plane defined by the *z*-axis and the axis of the trochlea. The direction is towards the radius.
y-axis: $z\text{-axis} \times x\text{-axis}$

Radius: center of the capitulum
 Origin: defined by the origin and the center of the scaphoid contact surface of the distal radius.
z-axis: The direction is from distal to proximal

x-axis: orthogonal to the z-axis and in the plane defined by the z-axis and the PS-axis i.e. the axis defined by the origin of the radial coordinate system and the center of the distal ulna. The direction is defined so that the scalar product between the x- and the PS-axis is negative
 y-axis: z-axis × x-axis
 Hand: rotational center of the radial-hand joint
 Origin: rotational center of the radial-hand joint

In order to be able to apply our results to other subjects as well, in the appendix we describe a simple method for scaling the integrals linearly and in the direction of the axes. Such scaling will give reasonable results if the ratio of circumferences of the forearm at wrist and elbow to the distance between the proc. Styloideus radii and the olecranon are close to the measurements of the forearm in this study, which were 17.5 cm : 26.5 cm : 26 cm.

3. Results

3.1. Dynamic and kinematic parameters of a male forearm

The angle between the z-x-planes of the ulna and radius was 79.5° for the intermediate position. The angles between the ulna and radius in the supinated and pronated position was $\Delta\alpha_1^0 = -44.8 \pm 2.4^\circ$ and $\Delta\alpha_1^0 = 70.5 \pm 1.2^\circ$, respectively.

In Table 1, we present the data resulting from the evaluation of the parameterized model for the arm studied in this article. As density of the forearm we assumed 1.14 g/cm (Drillis and Contini, 1966; Contini, 1972; Winter, 1990). The center of masses and the normalized principal axes of the inertia tensor of each segment are given with respect to the respective anatomical coordinate system.

The kinematic connection between the segments is established by giving the origin of the distal segment in coordinates of the proximal segment, i.e. giving the radial origin in ulnar and the hand origin in radial coordinates.

Radial origin: (0.0213, 0.0017, -0.0170)_{uln}.

Hand origin: (-0.0036, 0.0006, -0.2611)_{rad}.

The direction of the axis between the radial and ulnar segment is given with respect to both the ulnar and the radial anatomical coordinate system.

Radial-ulnar-axis: (0.0889, 0.0070, 0.9960)_{uln} = (0.0829, 0.0000, 0.9966)_{rad}.

4. Discussion

4.1. Discussion of the errors

The errors that possibly contributed to the differences between the two voxel-based partitions were numerous. They included magnetic field inhomogeneities, deformation of the arm because of its placement in a cushion, eventual movements of the arm during recording, the discrete nature of the mapping, the suppositions for the rotational movement, and inaccuracies in the determination of the PS-axis. However, the error of the mass of the radial segment can be estimated by the 4.6% difference between the number of voxels that were attributed to it by either mapping. Correspondingly, the 5.8% difference between the weighted G-values is a direct estimation for the error of the component of the inertia tensor in the direction of the PS-axis. These small differences show that within a range of $44.9^\circ + 70.5^\circ = 115.5^\circ$, our rigid body model represents a good approximation for the PS.

An additional error is made by the parameterization. Because of the parameterization, 6.8% of the radial segment voxels that were a result of the voxel-based partition were attributed to the ulnar segment and vice versa. However, it can be expected that smoothing the voxel-based partition's rough borders, which were at least partly the result of the discrete mapping process, would rather reduce the error of the voxel-based partition in the sense of a regression. Last but not least, because of the

Table 1
 Integrals of the dynamic quantities, i.e. mass, center of mass and inertia tensor, resulting from the evaluation of the parameterized model for the arm studied in this article. The center of mass and the normalized principal axes of the inertia tensors of each segment are given in the respective anatomical coordinate system

	Ulnar segment	Radial segment
Mass (kg)	0.970	0.205
Center of mass (m)	(0.0050, 0.0075, -0.0951)	(0.0116, 0.0033, -0.1881)
Normalized principal axes of the inertia tensors	$\begin{pmatrix} 0.9971 & -0.0355 & 0.0679 \\ 0.0319 & 0.9981 & 0.0535 \\ -0.0696 & -0.0511 & 0.9963 \end{pmatrix}$	$\begin{pmatrix} 0.9683 & -0.2139 & 0.1293 \\ 0.2231 & 0.9728 & -0.0617 \\ -0.1126 & 0.0886 & 0.9897 \end{pmatrix}$
Length of the principal axes of the inertia tensors (kg m ²)	(4.211, 4.373, 0.6741) × 10 ⁻³	(3.598, 3.323, 0.6175) × 10 ⁻⁴

smoothness of G as function of the cut-off value, such erroneous attribution results in a much smaller error for the kinetic energy.

We therefore estimate the error value for the integrals evaluated by the Monte-Carlo-integration of the parameterization of the forearm to be approximately 5%.

Another source of error was the impossibility of recording the elbow joint in the MRI-scans. The repeated fitting of the bony surfaces of the MRI-data onto a commercial bone polygon set to augment the geometrical data resulted in a standard deviation of 5° for the direction of the axis of the trochlea. The resulting error for the size of the main axes of the inertia tensor is negligible because of its high degeneracy in the x - and y -direction.

One flaw of this study could have resulted from the method of using the kinetic energy of a slowly rotating body to determine its dynamic integrals, which in turn are to be used in simulations of accelerated fast movements. If the shear modulus of the forearm were low, i.e. if the forearm tissue were very elastic, this would be indeed the case. Then radial torques within the physiologic range would elicit large local displacements without much effect on neighboring structures because of low shearing forces. Consequently, the movement angle $\Delta\alpha$ of a voxel would not be a unique function of the angle of rotation of the bony radius $\Delta\alpha^0$ as is assumed in this study, but would also depend on the angular velocity and acceleration. Fortunately, the anatomy of the forearm supports the contrary. As we have shown, the rotational component of the tissue movement is by far the most dominating component. The incompressibility of the tissue, together with the longitudinal structures that keep the anatomy in place during fast PS, e.g. the interossea membrane, guarantee that the dependence of $\Delta\alpha$ on angular velocity and acceleration can safely be neglected even for accelerated fast movements (within the physiologic range).

4.2. Discussion of the results

The construction of our forearm model is based on a number of assumptions: constant density of tissue, relevance of kinetic energy for the partitioning of body masses, and a fixed rotational axis in both the radial and the ulnar coordinate systems. As there is only one axis between the radial and the ulnar segment, it seems reasonable to choose this axis as the symmetry axis for the border surface of the two bodies. This would facilitate constructing a physical model of both segments such that they would not penetrate each other during rotation. However, such restriction would have resulted in an anatomically incorrect representation of the shape of the articulations between ulna and radius. At the elbow, the rotation of tissue takes place around the caput radii, i.e.

the articulation surface of the ulna is concave, while at the wrist the rotation takes place around the distal caput ulnae, i.e. the articulation surface of the ulna is convex. Consequently, the sign of the curvature of the border surface changes between wrist (cf. Fig. 4, slice 2) and elbow (cf. Fig. 4, slice 14). We therefore decided to respect the anatomy rather than to aim at a simple physical model.

It should be noted that for dynamic simulation the actual shapes of the simulated bodies are irrelevant because they do not appear in the differential equations of movement. As any inertia tensors could be produced by an infinite number of mass arrangements, a physical model of the forearm that would not interface with rotation can nevertheless be build on the basis of our dynamical parameters.

As we have shown, the mass between the radial and ulnar segment is ca. 1 : 4.5, whereas the relation between their inertia-tensors is ca. 1 : 11. It is obvious from these numbers that an approach that merges radius and ulna into a single segment rotating around the longitudinal axis would considerably overestimate the inertia during PS.

Furthermore, our study underlines the predominance of hand inertia in comparison to forearm inertia during PS movements. Hatze (1982) cites an inertia for a rotation of the hand around its long axis (for a male adult subject) as being approximately twice the value that we arrived at for the radial segment. Consequently, at least two thirds of the kinetic energy of the PS (depending on hand orientation) are stored in the hand. The inertia of the hand for a PS can be minimized by locating the center of mass onto the rotational axis, i.e. by a small abduction of the hand. Such abduction can actually be observed as a spontaneous adjustment which people show if they are asked to pronate/supinate as fast as possible. On the other hand, it can also be inferred that the radial inertia is still too large to justify a total neglect in any arm movements with an appreciable PS component.

If the data are used for simulations of arm movements in three dimensions, another property of the inertia tensors should be noted. In both tensors the principal axis in the longitudinal direction is smaller than the principal axes in the transversal direction by a factor of ca. 6, while the transversal axes are quite similar. Hence, when the principal axes are used to define a new coordinate system, as is often done to accelerate dynamical simulations, the coordinate system could be rotated arbitrarily around this longitudinal axis, resulting in only small errors.

Future developments might use new techniques in the area of fast elastic alignment (Schormann et al., 1996) to automatize the matching process, or could determine the velocity fields that are necessary to determine the kinetic energy for the partition in vivo by cine phase contrast

MRI, as was done by Sheehan et al. (1998) for the knee joint.

In summary, this study may be seen from two viewpoints. From a model builders' perspective it presents an interesting way to adapt (and evaluate) a rigid body model to a problem of continuum mechanics. It would be desirable for this method to be applied to other parts of the body that are similarly hard to parameterize, such as the shoulder region. From the perspective of someone who wants to simulate arm movements, this study provides the necessary data for the numerical calculation of arm dynamics.

Acknowledgements

We gratefully thank Prof. Dr. H.-J. Freund and Dr. H. Hefter of the Department of Neurology, University of Düsseldorf, Germany who made the MRI scans possible for us, and Mrs. B. Aldinger for her comments on this paper's english.

Appendix A. Scaling along the ulnar axes

If a scaling between two different bodies **B** and **B'** in the same coordinate system is performed along the coordinate axes, the dynamic parameters of both bodies, i.e. the masses *m* and *m'*, the center of masses **r_{cm}** and **r'_{cm}**, and the moments of inertia **J** and **J'** obey some simple rules.

In general, the assumption of a linear relationship between both bodies implies that each vector **r'**, of the body **B'** is related to a vector **r** of the body **B** by a constant 3 × 3 Matrix **E**

$$\mathbf{r}' = \mathbf{E}\mathbf{r}. \tag{A.1}$$

Therefore, given *m*, **r_{cm}**, and **J**, *m'*, **r'_{cm}**, and **J'** result from

$$m' = \int_{V'} dm' = \int_V |\mathbf{E}| dm = |\mathbf{E}|m, \tag{A.2}$$

$$\mathbf{r}'_{cm} = \frac{\int_{V'} \mathbf{r}' dm'}{m'} = \frac{\int_V \mathbf{E}\mathbf{r} |\mathbf{E}| dm}{|\mathbf{E}|m} = \mathbf{E}\mathbf{r}_{cm}, \tag{A.3}$$

$$\begin{aligned} \mathbf{J}' &= \int_{V'} r'^2 \mathbf{I}_3 - \mathbf{r}'\mathbf{r}'^T dm', \\ &= \int_V \mathbf{r}^T \mathbf{E}^T \mathbf{E} \mathbf{r} \mathbf{I}_3 - \mathbf{E}\mathbf{r}\mathbf{r}^T \mathbf{E}^T |\mathbf{E}| dm. \end{aligned} \tag{A.4}$$

As **E** is not unitarian, i.e. $\mathbf{E}^{-1} \neq \mathbf{E}^T$, the inertia tensor does not transform as $\mathbf{J}' = \mathbf{E}\mathbf{J}\mathbf{E}^T$. Instead, Eq. (A.4) has to be evaluated directly.

If the scaling is performed only along the coordinate axis of the bodies, i.e. when **E** is diagonal, all components of **J'** can be expressed in terms of the components of **J**. In this case the determinant is

$$|\mathbf{E}| = e_{11}e_{22}e_{33}. \tag{A.5}$$

The nondiagonal elements are given by

$$\begin{aligned} J'_{12} &= J'_{21} = e_{11}e_{22}|\mathbf{E}|J_{12}, \\ J'_{13} &= J'_{31} = e_{11}e_{33}|\mathbf{E}|J_{13}, \\ J'_{23} &= J'_{32} = e_{22}e_{33}|\mathbf{E}|J_{13}, \end{aligned} \tag{A.6}$$

and the diagonal elements by

$$\begin{pmatrix} J'_{11} \\ J'_{22} \\ J'_{33} \end{pmatrix} = \frac{|\mathbf{E}|}{2} \begin{pmatrix} e_{22}^2 + e_{33}^2 & -e_{22}^2 + e_{33}^2 & e_{22}^2 - e_{33}^2 \\ -e_{11}^2 + e_{33}^2 & e_{11}^2 + e_{33}^2 & e_{11}^2 - e_{33}^2 \\ -e_{11}^2 + e_{22}^2 & e_{11}^2 - e_{22}^2 & e_{11}^2 + e_{22}^2 \end{pmatrix} \begin{pmatrix} J_{11} \\ J_{22} \\ J_{33} \end{pmatrix}. \tag{A.7}$$

References

An, K.N., Hui, F., Morrey, B., Linscheid, R., et al., 1981. Muscles across the elbow joint: a biomechanical analysis. *Journal of Biomechanics* 14 (10), 659–669.

Chadwick, E., McCormack, B., Nicol, A.C., Peterson, B. et al., 1996. ISB-proposal for standardization of segmental coordinates — elbow joint, <http://www.kin.ucalgary.ca/isb/standards/elbow.html>.

Chao, E., Morrey, B., 1978. Three-dimensional rotation of the elbow. *Journal of Biomechanics* 11, 57–73.

Contini, R., 1972. Body segment parameters II. *Artificial Limbs* 16, 1–19.

Drillis, R., Contini, R., 1966. Body Segment Parameters. Report 1163-03, Office of Vocational Rehabilitation, Department of Health, Education and Welfare, New York.

Fick, 1911. *Anatomie und Mechanik der Gelenke Bd 3*. Gustav Fisher, Jena.

Hatze, H., 1980. A mathematical model for the computational determination of parameter values of anthropometric segments. *Journal of Biomechanics* 13, 833–843.

Hatze, H., 1982. HOMSIM. A simulator of spatial (3D) hominoid dynamics. BIOMLIB TR-82-UM-902.

Martin, P., Mungoile, M., Marzke, M., Longhill, J., 1989. The use of magnetic resonance imaging for measuring segment inertial properties. *Journal of Biomechanics* 22 (4), 367–376.

Murray, W.M., Delp, S.L., Buchanan, T.S., 1995. Variation of muscle moment arms with elbow and forearm position. *Journal of Biomechanics* 28 (5), 513–525.

Nigg, B.E., Herzog, W. (Eds.), 1999. *Biomechanics of the Musculoskeletal System*, 2nd Edition. Wiley, New York.

Peterson, B., 1994. On a model of the upper extremity. In: Schuind, F., et al. (Ed.), *Advances in the Biomechanics of the Hand and Wrist*. Plenum Press, New York, pp. 95–106.

Robin, M., An, K., Linscheid, R., Ritman, E., 1986. Anatomic and kinematic analysis of the human forearm using high-speed computed tomography. *Medical and Biological Engineering and Computation* 24, 164–168.

- Schormann, T., Henn, S., Zilles, K., 1996. A new approach to fast elastic alignment with applications to human brains. In: Söhne, K.H., Kikinis, R. (Eds.), *Lecture Notes in Computer Science* Vol. 1131. Springer, Berlin, pp. 337–342.
- Sheehan, F., Zajac, F., Drace, J., 1998. Using cine phase contrast magnetic resonance imaging to non-invasively study in vivo knee dynamics. *Journal of Biomechanics* 31, 21–26.
- Winter, D.A., 1990. *Biomechanics and Motor Control of Human Movement*. Wiley, New York.
- Youm, Y., Dryer, R., Thambyrajah, K., Flatt, A.E., et al., 1979. Biomechanical analyses of forearm pronation-supination and elbow flexion-extension. *Journal of Biomechanics* 12, 245–255.